

# FUTURE-VLA: Forecasting Unified Trajectories Under Real-time Execution

Jingjing Fan <sup>\*1</sup> Yushan Liu <sup>\*2</sup> Shoujie Li <sup>3</sup> Botao Ren <sup>1</sup> Siyuan Li <sup>4</sup> Xiao-Ping Zhang <sup>2</sup>  
Wenbo Ding <sup>2</sup> Zhidong Deng <sup>1</sup>

## Abstract

General vision-language models increasingly support unified spatiotemporal reasoning over long video streams, yet deploying such capabilities on robots remains constrained by the prohibitive latency of processing long-horizon histories and generating high-dimensional future predictions. To bridge this gap, we present FUTURE-VLA, a unified architecture that reformulates long-horizon control and future forecasting as a monolithic sequence-generation task. Adopting a dual-sided efficiency paradigm, FUTURE-VLA leverages a temporally adaptive compression strategy to maximize spatiotemporal information density, enabling the ingestion of extensive multi-view histories while maintaining constant inference latency. Simultaneously, it performs latent-space autoregression to align actionable dynamics with reviewable visual look-aheads in a single forward pass. These real-time predictive capabilities further enable a prediction-guided Human-In-the-Loop mechanism via interactive execution gating, allowing operators to dynamically validate behaviors based on interpretable future previews. Extensive evaluations demonstrate that FUTURE-VLA establishes new state-of-the-art performance, attaining success rates of 99.2% on LIBERO, 75.4% on RoboTwin, and 78.0% on a real-world Piper platform, all with a  $16 \times$  extended spatiotemporal window while maintaining the inference latency of a single-frame baseline. Project repo: [FUTURE-VLA Repo](#)

<sup>1</sup>Department of Computer Science and Technology, Tsinghua University <sup>2</sup>Shenzhen International Graduation School, Tsinghua University <sup>3</sup>School of Mechanical and Aerospace Engineering, Nanyang Technological University <sup>4</sup>Department of Automation, Tsinghua University. Correspondence to: Wenbo Ding <[ding.wenbo@sz.tsinghua.edu.cn](mailto:ding.wenbo@sz.tsinghua.edu.cn)>, Zhidong Deng <[michael@tsinghua.edu.cn](mailto:michael@tsinghua.edu.cn)>.

Preprint. February 19, 2026.

## 1. Introduction

In recent years, robot policy learning based on Vision-Language Models (VLMs) has witnessed significant progress. By building upon pre-trained general VLMs and incorporating large-scale physical interaction data, Vision-Language-Action (VLA) models and World Models (WMs) have progressively bridged the gap between linguistic instructions, visual observations, physical actions, and world dynamics (Kim et al., 2025; Li et al., 2025a; Lu et al., 2025; Guo et al., 2025; Chen et al., 2025c).

However, the prevailing paradigm remains dominated by modular fragmentation. As illustrated in Fig. 1(a), isolated VLA and WM systems suffer from representational mismatch, leading to pronounced perceptual myopia (Zhu et al., 2025; Li et al., 2025b). Under strict real-time constraints, the absence of efficient spatiotemporal compression makes processing long-horizon history computationally prohibitive without incurring severe latency penalties. Consequently, existing systems are forced into a suboptimal trade-off between preserving temporal context and maintaining response speed (Pei et al., 2025; Xu et al., 2025). Furthermore, the coordination between prediction and decision-making is constrained by excessive computational overhead. Even in preliminary unified architectures (Fig. 1 (b)), the system is typically restricted to single-frame output for visual reasoning, failing to fully exploit the anticipatory power of world models (Qi et al., 2025). Since conventional WMs rely on high-dimensional pixel-level rollouts, they cannot match the real-time frequency required for synchronous action chunking. This predictive fragmentation prevents the world model from providing practical online guidance during inference (Agarwal et al., 2025).

To address these challenges, we propose FUTURE-VLA, a unified architecture explicitly designed for "spatial-temporal unification" (Fig. 1(c)). On the input side, we introduce a spatiotemporal compression paradigm that maximizes information density under a fixed computational budget, enabling efficient long-context modeling. On the output side, we abandon expensive pixel-level rollouts in favor of autoregressive prediction in a highly compact latent space. This design enables the model to produce executable long-horizon action chunks along with their corresponding future state evolutions in a single forward pass.



Figure 1. Comparison of VLA-VM Architectures. (a) Modular Fragmentation: Independent VLA and World Model operating with decoupled representations. (b) Instantaneous Unification: A unified framework integrating perception and prediction within a short-horizon temporal window. (c) FUTURE-VLA (Ours): A spatiotemporally unified architecture that synchronously generates action chunks and future previews via latent-space autoregression in a single forward pass.

Leveraging its real-time predictive capabilities, our architecture facilitates a prediction-guided Human-In-the-Loop (HIL) paradigm. FUTURE-VLA generates action proposals alongside visual previews of their consequences in real-time, enabling human operators to employ an interactive execution gating strategy. In this way, the WM transforms from a passive training signal into a practically effective guidance module, improving task success rates and safety across diverse scenarios while preserving real-time performance.

We substantiate our contributions through extensive evaluations on the LIBERO benchmark, RoboTwin suite, and a real-world Piper platform. FUTURE-VLA establishes new state-of-the-art performance, attaining success rates of 99.2%, 75.4%, and 78.0%, respectively. These results confirm that our dual-sided efficiency paradigm successfully extends the bidirectional spatiotemporal window by 16 $\times$  while maintaining the inference latency of a single-frame baseline.

In summary, the main contributions of this paper are as follows:

- We propose a constrained-budget spatiotemporal compression paradigm that enables efficient long-horizon perception by maximizing information density within a fixed token budget.
- We present FUTURE-VLA, a unified framework that employs latent-space autoregression to synchronize action chunking and future prediction in a single forward pass without computational overhead.
- We develop a prediction-guided HIL mechanism, leveraging real-time future previews to implement dynamic execution gating for enhanced safety in robotic deployments.

## 2. Related Works

### 2.1. Visual-Language-Action

Pretrained vision–language models endow robots with strong semantic alignment and transferable representations. Building on these pretrained multimodal backbones, end-to-end paradigms that jointly align Visual on robot trajectories have emerged as a dominant route toward general-purpose robotic policies (Zitkovich et al., 2023; Kim et al., 2024; Pertsch et al., 2025). Prior methods include: discretizing continuous actions and learning policies as autoregressive sequences; scaling up with diverse robot datasets across tasks and embodiments to improve generalization (O’Neill et al., 2024; Liu et al., 2023; Team et al., 2024); adopting diffusion- or flow-based generative policies to better capture multi-modal action distributions and support long-horizon action generation (Chi et al., 2025; Black et al., 2025; Zhang et al., 2025b); and so on.

### 2.2. World Models for Robotics

World models learn action-conditioned predictive dynamics for imagination and long-horizon decision making, and with advances in video generation they increasingly act as generative, interactive simulators. Action-conditioned generative video models synthesize future observations with improved fidelity and temporal coherence for long rollouts (Rigter et al., 2024; Lou et al., 2025; Alonso et al., 2024), while controllable variants enforce multi-view consistency and long-horizon reliability via memory/retrieval or global-state conditioning, enabling policy-in-the-loop evaluation and data synthesis (Jiang et al., 2025; Ren et al., 2025). Self-supervised video representation learning provides general spatiotemporal features that can be aligned to action-controllable dynamics with limited interaction data (Wang et al., 2024; Assran et al., 2025); goal-conditioned compositional world modeling further adds factorized generation and multimodal constraints to generalize under novel compositions (Zhou et al., 2024b; Bruce et al., 2024). These models can also support online planning/MPC by sampling

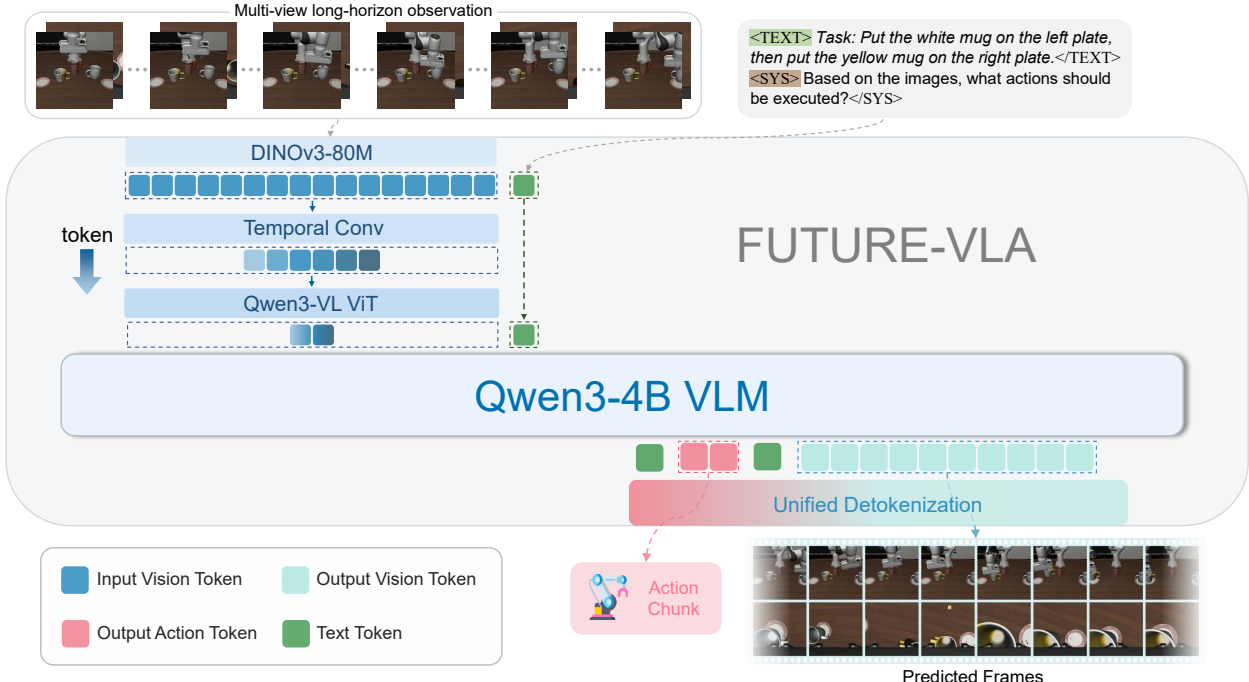


Figure 2. The architecture of FUTURE-VLA. On the input side, multi-view historical observations are encoded via a frozen DINOv3 encoder and processed through Temporally Adaptive Cascaded Compression to maximize information density under a fixed token budget. On the output side, the model autoregressively generates action chunks (via FAST spectral tokenization) and future visual predictions (via compact 1D tokenization with 32 tokens per frame) in a single forward pass.

and filtering candidate futures (Zhou et al., 2024a), and benchmarks increasingly emphasize long-horizon procedural reasoning and world consistency (Chen et al., 2025a).

Despite this progress, long-horizon multi-view control still faces persistent bottlenecks: extending history and viewpoints for robustness quickly explodes visual-token counts and inference cost (Tan et al., 2025; Wang et al., 2025), while open-loop execution of action chunks without predictive look-ahead tends to accumulate errors and drift over time (Xue et al., 2025; Sendai et al., 2025). For world models, the bottleneck is no longer forecasting itself but delivering controllable look-ahead under tight token/latency budgets (Po et al., 2025; Zhang et al., 2025a); high-fidelity multi-view rollouts remain compute-prohibitive, and loose coupling (WM as offline generator/evaluator, policy as executor) limits utility for high-rate closed-loop control (Bar et al., 2025).

To address them, we propose FUTURE-VLA, a unified architecture that enforces a dual-sided efficiency paradigm. By integrating budget-constrained spatiotemporal compression with latent-space autoregression, our model synchronizes action chunking and future prediction in a single forward pass. This real-time capability facilitates a prediction-guided HIL mechanism, ensuring safety in long-horizon tasks without computational penalties.

### 3. Method

We present FUTURE-VLA, a unified VLA framework that synergizes robotic control with world modeling capabilities. Figure 2 shows that FUTURE-VLA, built on Qwen3-VL (Bai et al., 2025), unifies closed-loop manipulation and future observation prediction into a single sequence-to-sequence generation problem. To address the computational challenges inherent in long-horizon interaction, we introduce a dual-sided efficiency strategy: on the input front, we employ a temporally adaptive compression mechanism to distill historical context while preserving critical spatial cues; on the output front, we map future observations to a compact discrete space. This minimal representation permits the efficient generation of visual dynamics that align precisely with the granularity of action chunks, ensuring the predicted world state evolves in lockstep with the control policy.

#### 3.1. Model Architecture

We re-engineer the visual encoding pathway of Qwen3-VL to capture long-horizon temporal dependencies, while fully harnessing the reasoning capabilities of the language backbone. Formally, the model ingests a multimodal context sequence defined as:

$$\mathbf{x} = [O_1; \dots; O_T; \text{TEXT}; \text{SYS}], \quad (1)$$

where  $O_i$  denotes the visual observation of the  $i$ -th historical frame, augmented by task-specific instructions (TEXT) and system prompts (SYS). Conditioned on this composite history, the model autoregressively yields a unified stream of action and future visual tokens.

**Visual Encoding & Cascaded Compression** To ensure strict geometric fidelity and object-centric correspondences, we substitute the native patch embedding with a frozen DINOv3-ViT-Base encoder (Siméoni et al., 2025). This backbone extracts dense, spatially discriminative feature maps essential for fine-grained manipulation. We explicitly discard the [CLS] and register tokens to focus exclusively on the 2D spatial grid, providing a structural foundation for precise physical interaction.

To address the context bottleneck inherent in long-horizon inputs, we introduce a Temporally Adaptive Cascaded Compression strategy. This approach balances long-term memory with short-term precision by applying a variable number of recursive compression blocks depending on the frame’s temporal distance.

First, we define the fundamental compression unit as a strided convolution followed by GeLU activation:

$$X^{(k)} = \text{GeLU}(\text{Conv}(X^{(k-1)})), \quad (2)$$

where the spatial resolution is updated recursively as  $(H_k, W_k) = (H_{k-1}/2, W_{k-1}/2)$ . Crucially, the compression depth  $k_t$  for a frame at time  $t$  is dynamic. We adopt a non-uniform tiered schedule where  $k_t$  is inversely proportional to the frame’s temporal proximity to the current step. This design heavily compresses distant history to maximize context length while preserving high-resolution spatial details for recent observations.

Second, these variable-resolution features are injected into the Qwen3-VL visual stack, which natively incorporates a patch merger with a merge size of  $2 \times 2$ . This built-in mechanism imposes a final, uniform  $4 \times$  reduction across all frames. By cascading our adaptive temporal compression with the backbone’s native merger, the system achieves a highly efficient representation that spans long horizons without overwhelming the context window.

### 3.2. Unified Tokenization

FUTURE-VLA operates in a unified vocabulary space by mapping discrete action and visual-latent codes onto the tail of the pre-trained Qwen3 tokenizer. This design avoids changing the tokenizer size and enables direct reuse of the original embedding matrix, while keeping the code tokens separated from commonly used text tokens during fine-tuning.

**Spectral Action Tokenization** For control signals, we leverage the FAST framework (Pertsch et al., 2025), which encodes trajectory chunks in the spectral domain via discrete cosine transform. This method prioritizes frequency components, allowing the model to capture high-frequency dynamics with substantial compression gains. This spectral approach ensures superior trajectory reconstruction while minimizing the sequence length required for complex maneuvers.

**Compact 1D Visual Tokenization** To facilitate efficient long-horizon prediction, we employ a 1D tokenizer architecture inspired by TiTok (Yu et al., 2024). Unlike standard VQ-GANs that enforce a rigid 2D spatial correspondence, this design decouples latent capacity from image resolution, representing each image with a fixed budget of 32 tokens.

Formally, an input image is patchified into a sequence of patch embeddings  $\mathbf{P}$  and concatenated with 32 learnable latent tokens  $\mathbf{L}$ . A ViT encoder processes the composite stream and aggregates visual information into the latents via attention. We retain only the latent outputs to obtain a compact 1D representation:

$$\mathbf{Z}_{1D} = \text{Enc}(\mathbf{P} \oplus \mathbf{L}) \in \mathbb{R}^{32 \times D}, \quad (3)$$

where  $\oplus$  denotes concatenation.

To enable autoregressive prediction, we discretize  $\mathbf{Z}_{1D}$  using a learned codebook  $\mathcal{E} \in \mathbb{R}^{|\mathcal{V}| \times D}$ . Specifically, the VLA predicts a length-32 sequence of discrete code indices  $\mathbf{c} \in \{1, \dots, |\mathcal{V}|\}^{32}$ , and obtains the quantized latents  $\tilde{\mathbf{Z}}_{1D}$  via codebook lookup, yielding  $\tilde{\mathbf{Z}}_{1D} = \mathcal{E}[\mathbf{c}]$ .

For image reconstruction, spatial geometry is restored by appending a grid of mask tokens  $\mathbf{M}$  as positional anchors for the target layout. The decoder then reconstructs the image from the quantized latents:

$$\hat{\mathbf{I}} = \text{Dec}(\tilde{\mathbf{Z}}_{1D} \oplus \mathbf{M}). \quad (4)$$

This design exploits patch-level redundancies to support high-fidelity reconstruction while maintaining an extremely lean token footprint for multi-step look-ahead.

### 3.3. Inference: Predictive Look-ahead

Leveraging the integrated world model, FUTURE-VLA implements a HIL Dynamic Execution strategy. As shown in Figure 3, the model generates an action chunk  $\mathbf{A}_{1:T}$  alongside a predicted visual trajectory  $\hat{\mathbf{O}}_{1:T}$ .

**Dynamic Gating** A verifier inspects  $\hat{\mathbf{O}}_{1:T}$  to determine a safe execution horizon  $k \in [1, T]$ . The robot executes  $k$  steps before refreshing observations, balancing open-loop speed with closed-loop safety.

**Resampling Recovery** If  $\hat{\mathbf{O}}_{1:T}$  suggests failure, the controller sets  $k=0$  (reject), executes no actions, and resamples

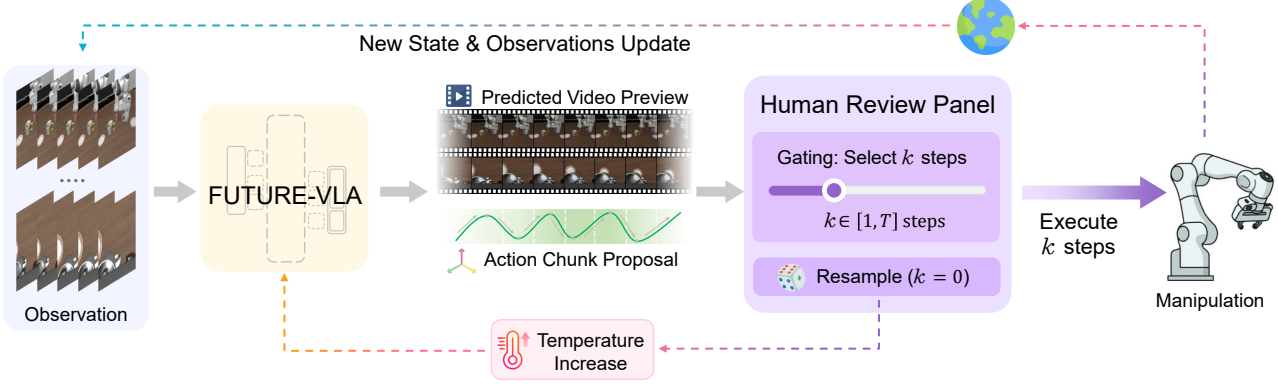


Figure 3. HIL Closed-Loop Execution with Resampling. FUTURE-VLA jointly generates action chunks and future visual previews, enabling a verifier to determine a safe execution horizon  $k$  via Dynamic Gating or reject erroneous proposals ( $k=0$ ) and trigger Resampling Recovery with increased temperature to escape deadlocks.

Table 1. LIBERO benchmark results (%). **Bold** values denote the best results, and underlined values denote the second-best.

MODEL	SPATIAL (%)	OBJECT (%)	GOAL (%)	LONG (%)	AVERAGE (%)
OPENVLA(KIM ET AL., 2024)	84.7	88.4	79.2	53.7	76.5
OPENVLA-OFT(KIM ET AL., 2025)	96.2	98.3	96.2	90.7	95.4
$\pi_0$ (BLACK ET AL., 2025)	96.8	98.8	95.8	85.2	94.2
$\pi_{0.5}$ (INTELLIGENCE ET AL., 2025)	<b>98.8</b>	98.2	<u>98.0</u>	<u>92.4</u>	<u>96.9</u>
$\pi_0$ +FAST(PERTSCH ET AL., 2025)	96.4	96.8	88.6	60.2	85.5
WORLDVLA(CEN ET AL., 2025)	87.6	96.2	83.4	60.0	81.8
<b>FUTURE-VLA (w/o HIL)</b>	89.6	<u>99.0</u>	95.2	81.2	91.3
<b>FUTURE-VLA (w/ HIL)</b>	<u>98.6</u>	<b>100</b>	<b>100</b>	<b>98.2</b>	<b>99.2</b>

with higher temperature to explore alternative trajectories and escape deadlocks.

## 4. Experiments

Our experiments are designed to investigate two primary aspects of the proposed method: (1) whether the incorporation of long-horizon visual history, enabled by our compressed DINOv3 representation, effectively enhances the accuracy of action prediction compared to standard short-context baselines; and (2) whether the proposed HIL strategy effectively benefits final task performance by mitigating potential execution failures.

### 4.1. Benchmarks and Experimental Setup

We conduct comprehensive evaluations across both simulation benchmarks and real-world scenarios to assess the model’s capabilities in single-arm manipulation, bimanual coordination, and long-horizon planning.

#### Simulation Benchmarks

- **LIBERO** (Liu et al., 2023) provides a suite of diverse manipulation tasks. We utilize the OpenPi LeRobot-formatted version and conduct experiments on all four sub-benchmarks: Libero-Spatial, Libero-Object,

Libero-Goal, and Libero-Long.

- **RoboTwin2.0** (Chen et al., 2025b) focuses on bimanual manipulation scenarios. We employ the Agilex Aloha dual-arm configuration on seven representative tasks, evaluating in unseen settings with randomized instructions, environmental textures, and object locations.

**Real-world Experiments** We conduct physical validation on an Agilex Piper dual-arm platform across three tasks of increasing hierarchical complexity. First, Target-Oriented Sorting assesses fine-grained manipulation and semantic grounding, requiring the robot to identify specific objects within a cluttered scene and place them into designated receptacles. Second, Collaborative Handover evaluates precise bimanual coordination, where the system must orchestrate an object transfer between arms to bridge spatially separated workspaces beyond single-arm reach. Finally, Table Cleanup tests long-horizon reasoning, demanding the autonomous chaining of sorting and handover primitives to clear multiple items from a chaotic environment. The detailed real-world setup is provided in Appendix A.

### 4.2. Implementation Details

**Model Configuration** Unless otherwise stated, we fix the input history length at  $T = 16$ . To optimize computational

Table 2. RoboTwin benchmark results. **Bold** values denote the best results, and underlined values denote the second-best.

MODEL	LIFT POT	BEAT HAMMER BLOCK	PLACE PHONE STAND	MOVE CAN POT
OPENVLA-OFT	9%	17%	13%	22%
$\pi_0$ +FAST	30%	38%	34%	51%
$\pi_{0.5}$	<b>44%</b>	<b>72%</b>	42%	<u>71%</u>
<b>FUTURE-VLA (w/o HIL)</b>	32%	63%	<u>48%</u>	<u>56%</u>
<b>FUTURE-VLA (w/ HIL)</b>	<u>38%</u>	<u>70%</u>	<b>66%</b>	<b>77%</b>

MODEL	HANOVER MIC	PICK DUAL BOTTLES	STACK BOWLS TWO	AVG (ALL)
OPENVLA-OFT	38%	32%	41%	24.6%
$\pi_0$ +FAST	83%	54%	62%	50.3%
$\pi_{0.5}$	<b>97%</b>	75%	74%	<u>67.9%</u>
<b>FUTURE-VLA (w/o HIL)</b>	88%	<u>83%</u>	<u>80%</u>	<u>64.3%</u>
<b>FUTURE-VLA (w/ HIL)</b>	<u>91%</u>	<b>92%</b>	<b>94%</b>	<b>75.4%</b>

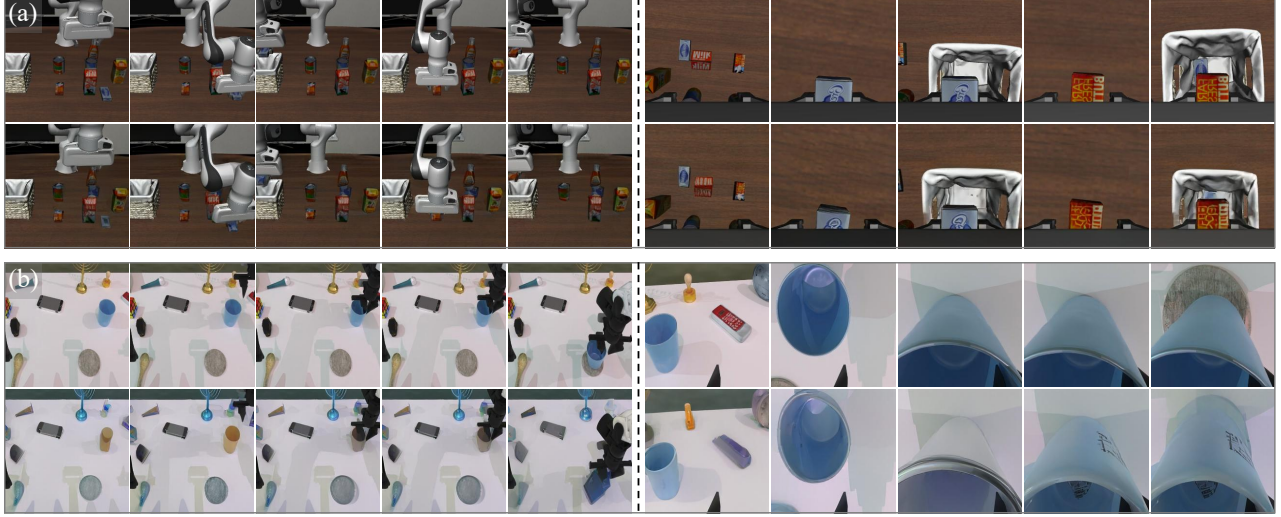


Figure 4. Multi-view rollout visualization in LIBERO and RoboTwin. Top: executed rollout keyframes (ground truth). Bottom: predicted future frames (time left to right).

efficiency, we employ a tiered compression strategy: the earliest 8, middle 6, and latest 2 frames are processed with 2, 1, and 0 compression blocks, yielding 4, 16, and 64 tokens per image, respectively. This aggregates to 256 tokens per view, allowing our 16-frame context to match the token budget of a standard single-frame baseline. For outputs, we align the action chunk size and future prediction horizon at  $H_a = 16$ . The visual head generates a sequence of  $V \times 16 \times 32$  tokens, where the view count  $V$  is set to 2 for LIBERO and 3 for RoboTwin and real-world tasks. Detailed data construction and training procedures are provided in Appendices B and C.

**Evaluation Protocol** We assess performance under two distinct protocols: Autonomous Execution, where the robot executes the full predicted action chunk open-loop; and human-in-the-loop, which leverages visual foresight for interactive guidance. To strictly benchmark the model’s intrinsic generation quality, all ablation studies (Sec. 4.5) are reported using the autonomous protocol.

### 4.3. Evaluation Results

As shown in Table 1, FUTURE-VLA demonstrates robust autonomous performance on the LIBERO benchmark, achieving a 91.3% average success rate without human intervention, thereby surpassing both OpenVLA and WorldVLA. Enabling HIL execution gating further elevates performance to a near-perfect 99.2%, establishing a new state-of-the-art. This substantial improvement confirms that our generated visual look-aheads effectively empower operators to preemptively filter erroneous trajectories before execution.

In the long-horizon RoboTwin suite (Table 2), where baseline models like OpenVLA-OFT falter (24.6%), FUTURE-VLA (w/ HIL) attains a superior 75.4% success rate, outperforming the strong  $\pi_{0.5}$  baseline (67.9%). Notably, our model dominates in precision-critical tasks, achieving 94% on “Stack Bowls” and 92% on “Pick Dual Bottles” (compared to 74% and 75% for  $\pi_{0.5}$ ). These results validate that our unified tokenization strategy effectively preserves the essential geometric fidelity required for delicate manipula-

Table 3. Real-world experiments results (%). **Bold** values denote the best results, and underlined values denote the second-best.

MODEL	SORTING (%)	HANOVER (%)	TABLE CLEANUP (%)	AVERAGE (%)
OPENVLA-OFT	68	26	6	33.3
$\pi_0$ +FAST	74	40	22	45.3
$\pi_{0.5}$	92	<b>72</b>	<u>58</u>	<u>74</u>
<b>FUTURE-VLA (w/o HIL)</b>	<b>96</b>	<u>66</u>	40	67.3
<b>FUTURE-VLA (w/ HIL)</b>	<b>98</b>	<b>72</b>	<b>64</b>	<b>78</b>

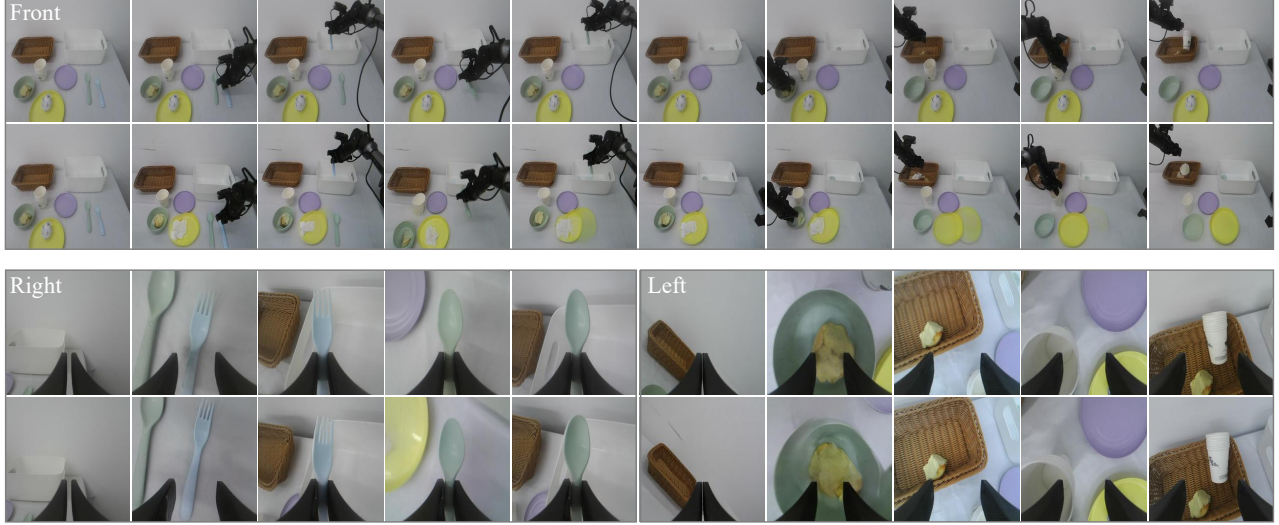


Figure 5. Multi-view rollout visualization in the real-world setup. Top: executed rollout keyframes (ground truth). Bottom: predicted future frames (time left to right).

 Table 4. Ablation study 1. Varying temporal horizon  $T$  under a fixed budget of 256 tokens/view.  $N_k$  denotes the frame count for compression stage  $k$ .

FRAME ALLOCATION ( $N_{k=2} : N_{k=1} : N_{k=0}$ )	SUCCESS RATE (%)
0 : 0 : 4 ( $T = 4$ )	86.0
0 : 8 : 2 ( $T = 10$ )	88.6
0 : 16 : 0 ( $T = 16$ )	81.5
<b>8 : 6 : 2 (<math>T = 16</math>)</b>	<b>91.3</b>
16 : 4 : 2 ( $T = 22$ )	83.1
32 : 0 : 2 ( $T = 34$ )	74.4

 Table 5. Ablation study 2. Varying compression strategies with fixed history length  $T = 16$ .  $N_k$  denotes the frame count for compression stage  $k$ .

FRAME ALLOCATION ( $N_{k=2} : N_{k=1} : N_{k=0}$ )	SUCCESS RATE (%)
16 : 0 : 0 (64 TOKS)	30.2
12 : 4 : 0 (112 TOKS)	65.4
0 : 16 : 0 (256 TOKS)	81.5
<b>8 : 6 : 2 (256 TOKS)</b>	<b>91.3</b>
8 : 4 : 4 (352 TOKS)	90.8
0 : 0 : 16 (1024 TOKS)	92.0

tion.

Finally, Table 3 reports performance in real-world manipulation tasks. FUTURE-VLA (w/ HIL) secures the highest average success rate of 78%, exceeding  $\pi_{0.5}$  (74%) and significantly outperforming OpenVLA-OFT (33.3%). Specifically for the multi-stage “Table Cleanup” task, HIL intervention boosts success from 40% to 64%, demonstrating the system’s capability to recover from physical disturbances via interactive guidance.

#### 4.4. Visualization

We provide qualitative visualizations of the proposed framework in simulation (Fig. 4) and real-world scenarios (Fig. 5). Fig. 4 illustrates tasks from the LIBERO (top panel) and RoboTwin (bottom panel) suites. Across all figures, for each view, the upper row displays the actual keyframes observed during evaluation rollouts, while the lower row presents the corresponding future frames predicted by the model. This alignment demonstrates the high fidelity of our autoregressive future prediction in guiding long-horizon execution. Additional demonstrations are presented in Appendix D.



Figure 6. Spatial Feature Visualization from DINOv3. From left to right: examples from Libero, RoboTwin, and Real-world domains. For each image, we select a query patch (black square) and compute the similarity between its feature and all other patches, shown as a heatmap. Warmer colors indicate higher similarity to the selected patch.



Figure 7. Visual Reconstruction via 1D-Tokenizer. From left to right: examples from Libero, RoboTwin, and Real-world domains. In each pair, we compare the ground-truth observation (left) with the reconstructed image (right) decoded from only 32 discrete tokens.

#### 4.5. Ablation Study

We investigate the design choices of FUTURE-VLA through a two-phase ablation, focusing on temporal horizon ( $T$ ) and token allocation strategy.

#### Trade-off between Temporal Horizon and Information Density

We first identify the optimal history length under a strict budget of 256 tokens per view (Table 4). The results exhibit an inverted U-shaped trend: extremely short horizons ( $T = 4$ ) suffer from insufficient temporal context (86.0%), while excessive extension ( $T = 34$ ) degrades performance to 74.4% due to aggressive compression of intermediate states. The proposed 8:6:2 configuration ( $T = 16$ ) strikes the optimal balance between context length and spatial precision, achieving a peak success rate of 91.3%.

**Efficiency of Hierarchical Compression** We further evaluate our adaptive token schedule against uniform baselines with a fixed horizon of  $T = 16$  (Table 5). Notably, our 8:6:2 strategy (256 tokens) yields performance comparable to the computation-heavy dense baseline (0:0:16, 1024 tokens), achieving 91.3% against 92.0% while reducing token consumption by 75%. In contrast, uniform heavy compression (16:0:0) leads to performance collapse (30.2%). This confirms that high-resolution retention is critical primarily for immediate observations, validating our temporal-resolution pyramid design.

#### 4.6. Analysis

**Spatial Feature Correspondence** We analyze the patch-level feature correlations to understand how our visual backbone supports manipulation tasks. As visualized in Figure 6,

the DINOv3-based features exhibit two critical spatial properties:

(1) **Precise Spatial Localization:** The heatmaps demonstrate sharp boundaries between objects and the workspace. Activation is strictly confined to the object instances with minimal leakage onto the tabletop background. This high object-background contrast is essential for precise picking and prevents collision with the environment.

(2) **Affordance-aligned Geometric Consistency:** Beyond category-level recognition, the features capture fine-grained spatial geometry. For instance, querying the handle of a fork specifically activates the geometrically similar handle of an adjacent spoon. This suggests the model learns part-level structural cues—aligning with graspable affordances—which enables the policy to generalize manipulation skills across objects with similar local geometries.

**Compact 1D-Tokenization** We evaluate the representation capability of our tokenizer, which compresses high-dimensional visual observations into a sequence of merely 32 discrete tokens. Figure 7 shows qualitative reconstructions, comparing the ground truth with the decoded outputs. Despite the extreme compression ratio, the reconstructed images preserve fine visual details with minimal perceptual deviation from the ground truth. This reconstruction quality is pivotal for the World Model: it helps keep generated future rollouts crisp and structurally consistent, providing the HIL policy with clear visual foresight for precise execution.

## 5. Conclusion

We have presented FUTURE-VLA, a unified architecture that resolves the spatiotemporal bottlenecks of robotic poli-

cies through a dual-sided efficiency paradigm. By integrating constrained spatiotemporal compression with latent-space autoregression, we extend the bidirectional context window by  $16\times$  while maintaining single-frame inference latency. Crucially, this real-time capability empowers a prediction-guided HIL mechanism, which establishes new state-of-the-art performance across diverse benchmarks by transforming world models into interpretable safety guardians for scalable embodied intelligence.

## Impact Statement

This paper presents work whose goal is to advance the field of Machine Learning. There are many potential societal consequences of our work, none of which we feel must be specifically highlighted here.

## References

Agarwal, N., Ali, A., Bala, M., Balaji, Y., Barker, E., Cai, T., Chattopadhyay, P., Chen, Y., Cui, Y., Ding, Y., et al. Cosmos World Foundation Model Platform for Physical AI. *arXiv preprint arXiv:2501.03575*, 2025.

Alonso, E., Jolley, A., Micheli, V., Kanervisto, A., Storkey, A. J., Pearce, T., and Fleuret, F. Diffusion for World Modeling: Visual Details Matter in Atari. *Advances in Neural Information Processing Systems*, 37:58757–58791, 2024.

Assran, M., Bardes, A., Fan, D., Garrido, Q., Howes, R., Muckley, M., Rizvi, A., Roberts, C., Sinha, K., Zhou, A., et al. V-JEPA 2: Self-Supervised Video Models Enable Understanding, Prediction and Planning. *arXiv preprint arXiv:2506.09985*, 2025.

Bai, S., Cai, Y., Chen, R., Chen, K., Chen, X., et al. Qwen3-VL Technical Report, 2025. URL <https://arxiv.org/abs/2511.21631>.

Bar, A., Zhou, G., Tran, D., Darrell, T., and LeCun, Y. Navigation World Models. In *Proceedings of the Computer Vision and Pattern Recognition Conference*, pp. 15791–15801, 2025.

Black, K., Brown, N., Driess, D., Esmail, A., Equi, M., Finn, C., Fusai, N., Groom, L., Hausman, K., Ichter, B., et al.  $\pi_0$ : A Vision-Language-Action Flow Model for General Robot Control. *arXiv preprint ArXiv:2410.24164*, 2025.

Bruce, J., Dennis, M. D., Edwards, A., Parker-Holder, J., Shi, Y., Hughes, E., Lai, M., Mavalankar, A., Steigerwald, R., Apps, C., et al. Genie: Generative Interactive Environments. In *Forty-first International Conference on Machine Learning*, 2024.

Cen, J., Yu, C., Yuan, H., Jiang, Y., Huang, S., Guo, J., Li, X., Song, Y., Luo, H., Wang, F., et al. WorldVLA: Towards Autoregressive Action World Model. *arXiv preprint arXiv:2506.21539*, 2025.

Chen, D., Chung, W., Bang, Y., Ji, Z., and Fung, P. World-Prediction: A Benchmark for High-Level World Modeling and Long-Horizon Procedural Planning. *arXiv preprint arXiv:2506.04363*, 2025a.

Chen, T., Chen, Z., Chen, B., Cai, Z., Liu, Y., Liang, Q., Li, Z., Lin, X., Ge, Y., Gu, Z., et al. RoboTwin 2.0:

A Scalable Data Generator and Benchmark with Strong Domain Randomization for Robust Bimanual Robotic Manipulation. *arXiv preprint arXiv:2506.18088*, 2025b.

Chen, Z., Huo, J., Chen, Y., and Gao, Y. RoboHorizon: An LLM-Assisted Multi-View World Model for Long-Horizon Robotic Manipulation. *arXiv preprint arXiv:2501.06605*, 2025c.

Chi, C., Xu, Z., Feng, S., Cousineau, E., Du, Y., Burchfiel, B., Tedrake, R., and Song, S. Diffusion Policy: Visuomotor Policy Learning via Action Diffusion. *The International Journal of Robotics Research*, 44(10-11): 1684–1704, 2025.

Guo, Y., Shi, L. X., Chen, J., and Finn, C. Ctrl-World: A Controllable Generative World Model for Robot Manipulation. *arXiv preprint arXiv:2510.10125*, 2025.

Intelligence, P., Black, K., Brown, N., Darpinian, J., Dhabalia, K., Driess, D., Esmail, A., Equi, M., Finn, C., et al.  $\pi_{0.5}$ : A Vision-Language-Action Model with Open-World Generalization. *arXiv preprint arXiv:2504.16054*, 2025.

Jiang, Z., Liu, K., Qin, Y., Tian, S., Zheng, Y., Zhou, M., Yu, C., Li, H., and Zhao, D. World4RL: Diffusion World Models for Policy Refinement with Reinforcement Learning for Robotic Manipulation. *arXiv preprint arXiv:2509.19080*, 2025.

Kim, M. J., Pertsch, K., Karamcheti, S., Xiao, T., Balakrishna, A., Nair, S., Rafailov, R., Foster, E., Lam, G., Sanketi, P., et al. OpenVLA: An Open-Source Vision-Language-Action Model. *arXiv preprint arXiv:2406.09246*, 2024.

Kim, M. J., Finn, C., and Liang, P. Fine-Tuning Vision-Language-Action Models: Optimizing Speed and Success. *arXiv preprint arXiv:2502.19645*, 2025.

Li, J., Zhu, Y., Tang, Z., Wen, J., Zhu, M., Liu, X., Li, C., Cheng, R., Peng, Y., Peng, Y., et al. CoA-VLA: Improving Vision-Language-Action Models via Visual-Text Chain-of-Affordance. In *Proceedings of the IEEE/CVF International Conference on Computer Vision*, pp. 9759–9769, 2025a.

Li, S., Gao, Y., Sadigh, D., and Song, S. Unified Video Action Model. *arXiv preprint arXiv:2503.00200*, 2025b.

Liu, B., Zhu, Y., Gao, C., Feng, Y., Liu, Q., Zhu, Y., and Stone, P. LIBERO: Benchmarking Knowledge Transfer for Lifelong Robot Learning. *Advances in Neural Information Processing Systems*, 36:44776–44791, 2023.

Lou, H., Liu, Y., Pan, Y., Geng, Y., Chen, J., Ma, W., Li, C., Wang, L., Feng, H., Shi, L., et al. Robo-gs: A physics consistent spatial-temporal model for robotic arm with hybrid representation. In *2025 IEEE International Conference on Robotics and Automation (ICRA)*, pp. 15379–15386. IEEE, 2025.

Lu, G., Jia, B., Li, P., Chen, Y., Wang, Z., Tang, Y., and Huang, S. GWM: Towards Scalable Gaussian World Models for Robotic Manipulation. In *Proceedings of the IEEE/CVF International Conference on Computer Vision*, pp. 9263–9274, 2025.

O’Neill, A., Rehman, A., Maddukuri, A., Gupta, A., Padalkar, A., Lee, A., Pooley, A., Gupta, A., Mandlekar, A., Jain, A., et al. Open X-Embodiment: Robotic Learning Datasets and RT-X Models. In *2024 IEEE International Conference on Robotics and Automation (ICRA)*, pp. 6892–6903. IEEE, 2024.

Pei, X., Chen, Y., Xu, S., Wang, Y., Shi, Y., and Xu, C. Action-Aware Dynamic Pruning for Efficient Vision-Language-Action Manipulation. *arXiv preprint arXiv:2509.22093*, 2025.

Pertsch, K., Stachowicz, K., Ichter, B., Driess, D., Nair, S., Vuong, Q., Mees, O., Finn, C., and Levine, S. FAST: Efficient Action Tokenization for Vision-Language-Action Models. *arXiv preprint arXiv:2501.09747*, 2025.

Po, R., Nitzan, Y., Zhang, R., Chen, B., Dao, T., Shechtman, E., Wetzstein, G., and Huang, X. Long-Context State-Space Video World Models. *arXiv preprint arXiv:2505.20171*, 2025.

Qi, H., Yin, H., Zhu, A., Du, Y., and Yang, H. Strengthening Generative Robot Policies Through Predictive World Modeling. *arXiv preprint arXiv:2502.00622*, 2025.

Ren, B., Hu, J., Xue, X., Luo, M., Chen, J., Bai, H., You, L., and Xu, M. Astranav-memory: Contexts compression for long memory. *arXiv preprint arXiv:2512.21627*, 2025.

Rigter, M., Gupta, T., Hilmkil, A., and Ma, C. AVID: Adapting Video Diffusion Models to World Models. *arXiv preprint arXiv:2410.12822*, 2024.

Sendai, K., Alvarez, M., Matsushima, T., Matsuo, Y., and Iwasawa, Y. Leave No Observation Behind: Real-Time Correction for VLA Action Chunks. *arXiv preprint arXiv:2509.23224*, 2025.

Siméoni, O., Vo, H. V., Seitzer, M., Baldassarre, F., Oquab, M., Jose, C., Khalidov, V., Szafraniec, M., Yi, S., Ramamonjisoa, M., et al. Dinov3. *arXiv preprint arXiv:2508.10104*, 2025.

Tan, X., Yang, Y., Ye, P., Zheng, J., Bai, B., Wang, X., Hao, J., and Chen, T. Think Twice, Act Once: Token-Aware Compression and Action Reuse for Efficient Inference in Vision-Language-Action Models. *arXiv preprint arXiv:2505.21200*, 2025.

Team, O. M., Ghosh, D., Walke, H., Pertsch, K., Black, K., Mees, O., Dasari, S., Hejna, J., Kreiman, T., Xu, C., et al. Octo: An Open-Source Generalist Robot Policy. *arXiv preprint arXiv:2405.12213*, 2024.

Wang, H., Xu, J., Pan, J., Zhou, Y., and Dai, G. SpecPrune-VLA: Accelerating Vision-Language-Action Models via Action-Aware Self-Speculative Pruning. *arXiv preprint arXiv:2509.05614*, 2025.

Wang, Y., Li, K., Li, X., Yu, J., He, Y., Chen, G., Pei, B., Zheng, R., Wang, Z., Shi, Y., et al. InternVideo2: Scaling Foundation Models for Multimodal Video Understanding. In *European Conference on Computer Vision*, pp. 396–416. Springer, 2024.

Xu, S., Wang, Y., Xia, C., Zhu, D., Huang, T., and Xu, C. VLA-Cache: Efficient Vision-Language-Action Manipulation via Adaptive Token Caching. In *The Thirty-ninth Annual Conference on Neural Information Processing Systems*, 2025.

Xue, H., Ren, J., Chen, W., Zhang, G., Fang, Y., Gu, G., Xu, H., and Lu, C. Reactive Diffusion Policy: Slow-Fast Visual-Tactile Policy Learning for Contact-Rich Manipulation. *arXiv preprint arXiv:2503.02881*, 2025.

Yu, Q., Weber, M., Deng, X., Shen, X., Cremers, D., and Chen, L.-C. An Image is Worth 32 Tokens for Reconstruction and Generation. *arXiv preprint arXiv:2406.07550*, 2024.

Zhang, P.-F., Cheng, Y., Sun, X., Wang, S., Li, F., Zhu, L., and Shen, H. T. A Step Toward World Models: A Survey on Robotic Manipulation. *arXiv preprint arXiv:2511.02097*, 2025a.

Zhang, Q., Liu, Z., Fan, H., Liu, G., Zeng, B., and Liu, S. FlowPolicy: Enabling Fast and Robust 3D Flow-Based Policy via Consistency Flow Matching for Robot Manipulation. In *Proceedings of the AAAI Conference on Artificial Intelligence*, volume 39, pp. 14754–14762, 2025b.

Zhou, G., Swaminathan, S., Raju, R. V., Guntupalli, J. S., Lehrach, W., Ortiz, J., Dedieu, A., Lázaro-Gredilla, M., and Murphy, K. Diffusion Model Predictive Control. *arXiv preprint arXiv:2410.05364*, 2024a.

Zhou, S., Du, Y., Chen, J., Li, Y., Yeung, D.-Y., and Gan, C. RoboDreamer: Learning Compositional World Models for Robot Imagination. *arXiv preprint arXiv:2404.12377*, 2024b.

Zhu, C., Yu, R., Feng, S., Burchfiel, B., Shah, P., and Gupta, A. Unified World Models: Coupling Video and Action Diffusion for Pretraining on Large Robotic Datasets. *arXiv preprint arXiv:2504.02792*, 2025.

Zitkovich, B., Yu, T., Xu, S., Xu, P., Xiao, T., Xia, F., Wu, J., Wohlhart, P., Welker, S., Wahid, A., et al. RT-2: Vision-Language-Action Models Transfer Web Knowledge to Robotic Control. In *Conference on Robot Learning*, pp. 2165–2183. PMLR, 2023.

## A. Real-world Experimental Setup

### A.1. Hardware Configuration

Our physical testbed relies on the Agilex Piper, a lightweight dual-arm manipulator system. Each arm possesses 6 degrees of Freedom (DoF) and a payload capacity of 1.5 kg, enabling flexible bimanual manipulation in restricted workspaces.

For visual perception, we construct a multi-view observation space using three RGB-D cameras. Specifically, an Intel RealSense D435i is mounted overhead to provide a global view of the workspace, while two additional cameras are attached to the wrists of the left and right arms to capture ego-centric views and mitigate occlusion. All RGB streams are captured at a resolution of  $640 \times 480$  to balance visual fidelity with computational efficiency.

The entire system is controlled via a central workstation powered by an NVIDIA RTX 4090 GPU (24 GB VRAM) to ensure real-time inference performance.

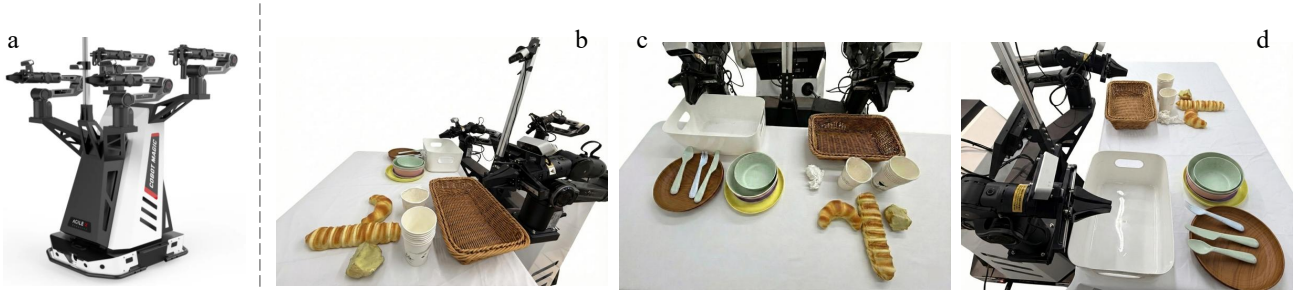


Figure 8. Real-world setup of our bimanual manipulation testbed. (a) Overview of the AgileX Piper dual-arm platform. (b) External view of the tabletop scene. (c) Front view of the workspace. (d) Side view of the workspace.

### A.2. Task Definitions

We designed three distinct tasks to evaluate FUTURE-VLA using a standardized set of everyday objects. As shown in the setup, the object set involves two categories: tableware (including stacked bowls, plates, and cutlery such as forks and spoons) and post-meal waste (including crumpled napkins, paper cups, and food scraps like baguettes and croissants).

#### A.2.1. TASK I: TARGET-ORIENTED SORTING

This task evaluates the model's semantic grounding and precision control. The workspace is populated with objects from both categories. Based on the semantic classification of the object, the robot acts to place tableware into the white bin and waste into the brown basket. The system must correctly identify the target item's category and execute a precise pick-and-place primitive to the corresponding receptacle.



Figure 9. Target-Oriented Sorting.

#### A.2.2. TASK II: COLLABORATIVE HANDOVER

This task assesses bimanual coordination for extending the effective workspace. In this scenario, a target object is deliberately placed out of the kinematic reach of the arm responsible for its destination container (e.g., a piece of trash located on the far right, while the trash basket is on the far left). The system must execute a multi-step strategy: the arm closest to the object first retrieves it and places it into a shared reachable region. Subsequently, the other arm grasps the object from this intermediate position and deposits it into the correct container.

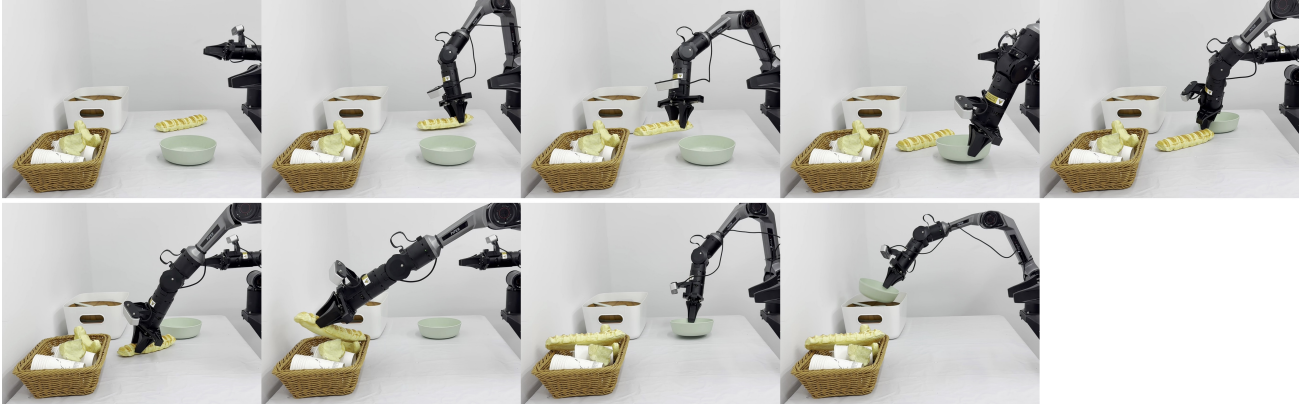


Figure 10. Collaborative Handover.

#### A.2.3. TASK III: LONG-HORIZON TABLE CLEANUP

The Table Cleanup task integrates the primitives from the previous tasks into a complex, long-horizon mission. The table is initialized with a chaotic arrangement of multiple tableware items and waste products. Given the high-level goal "Clean up the table," the robot must autonomously perform a chain of decisions. It needs to sequentially identify objects, decide whether a direct sort (Task I) or a collaborative transfer (Task II) is required based on the object's location, and continuously execute these actions until the workspace is clear.



Figure 11. Table Cleanup.

## B. Data Construction

In this section, we detail the data preparation pipelines for both the visual tokenizer and the main FUTURE-VLA model.

### B.1. Data for Compact 1D Visual Tokenizer

To support robust visual encoding, we trained two distinct tokenizer models tailored to different domains: one unified model for the simulation environments (covering both LIBERO and RoboTwin benchmarks) and a separate model for the real-world environment. For training data, we utilized all available camera frames captured during data collection, irrespective of whether the specific frames were used in the final behavioral cloning sequences. This strategy maximizes the diversity of visual patterns the tokenizer is exposed to. All images were resized to a resolution of  $256 \times 256$  to match the model’s input specifications.

### B.2. Data for FUTURE-VLA

For the main policy learning, we trained three separate models corresponding to the three experimental scenarios (LIBERO, RoboTwin, and Real-world). The data construction involves sequence formatting and a specialized vocabulary adaptation strategy.

**Sequence Formulation** We formulate the training data as a multimodal sequence generation task with a context window of  $T = 16$  steps.

- Input: A sequence of  $T$  multi-view image groups, a system prompt, and a natural language instruction. The number of camera views is set to 2 for LIBERO and 3 for both RoboTwin and the Real-world setup.
- Output: A textual transition string, a sequence of discrete action tokens (FAST codes), and the predicted future  $T$  image groups (as 1D visual-token sequences).

We apply a sliding window with stride 1 to generate training samples. For sequences shorter than  $T$ , we pad by replicating the first/last frame to maintain consistent temporal dimensions.

**Vocabulary Expansion and Tokenization** We employ the following strategies:

1. Discretization: We utilize the FAST action encoder with a vocabulary size of  $V_{act} = 2048$  to discretize continuous actions. Visual observations are tokenized using our pre-trained Compact 1D Visual Tokenizer, which has a vocabulary size of  $V_{vis} = 4096$ .
2. Special Tokens: We introduce four new special tokens to the Qwen3 vocabulary to serve as delimiters, wrapping each action token group and each image’s sequence of 32 tokens. This structural marking aids the model in distinguishing between modalities.
3. Vocabulary Remapping Strategy: Instead of expanding the vocabulary with randomly initialized embeddings, we adopt a remapping strategy to utilize the existing semantic space. We map the action tokens to the last 2048 indices of Qwen’s original vocabulary. Similarly, the visual tokens are mapped to the 4096 indices immediately preceding the action tokens. Since Qwen utilizes Byte-Pair Encoding (BPE), the tokens at the tail of the vocabulary typically correspond to extremely rare character sequences in natural language. We posit that repurposing these low-frequency slots minimizes interference with the pre-trained linguistic knowledge while allowing the model to learn modality-specific representations.

**Training Format** The final training instances are formatted as: [16 Input Image Groups, Instruction, System Prompt]  $\rightarrow$  [Transition Text, Token Sequence]. Notably, using the ms-swift framework, we bypass the standard text tokenizer for the output targets. Instead, we directly feed the pre-computed action and visual token IDs into the label sequence. This ensures that the specific discrete codes are optimized directly without being re-encoded into UTF-8 strings.

## C. Train Details

### C.1. Training of Compact 1D Visual Tokenizer

Following the official implementation of TiTok (Yu et al., 2024), we adopt a two-stage training strategy to decouple structure learning from texture reconstruction. In the first stage, the tokenizer is trained to predict proxy codes generated by a pre-trained MaskGIT-VQGAN, serving as a structural warm-up. In the second stage, the decoder is fine-tuned to minimize the pixel-level reconstruction loss, ensuring high visual fidelity. While the original configuration employs a larger batch size, we constrained the global batch size to 256 (implemented as 32 per GPU across 8 GPUs) for both stages to accommodate our hardware constraints. Apart from the batch size, we adhere to the original hyperparameter settings, including the optimizer choice, learning rate schedules, and loss weighting strategies provided in the official repository.

### C.2. Training of FUTURE-VLA

For the main VLA model, we implemented the training pipeline using the `ms-swift` framework. We employed the AdamW optimizer, a standard choice for large-scale supervised fine-tuning (SFT), configured with  $\beta_1 = 0.9$ ,  $\beta_2 = 0.999$ , and a numerical stability term  $\epsilon = 1e-8$ . We applied a weight decay of 0.1 to regularize the model parameters. The learning rate followed a cosine decay schedule with a linear warm-up. Specifically, the learning rate increases linearly to a peak of  $1 \times 10^{-4}$  during the warm-up phase and then decays according to a cosine curve over the course of 2 training epochs. A global batch size of 64 was maintained to ensure stable gradient estimation.

## D. Additional Visualization

In this section, we provide comprehensive visualization results from our real-world experiments. Figures 12–18 illustrate additional execution trajectories. These visualizations further demonstrate FUTURE-VLA’s capability to generalize across a diverse set of unseen tableware and waste objects, as well as its robustness in handling cluttered spatial arrangements.

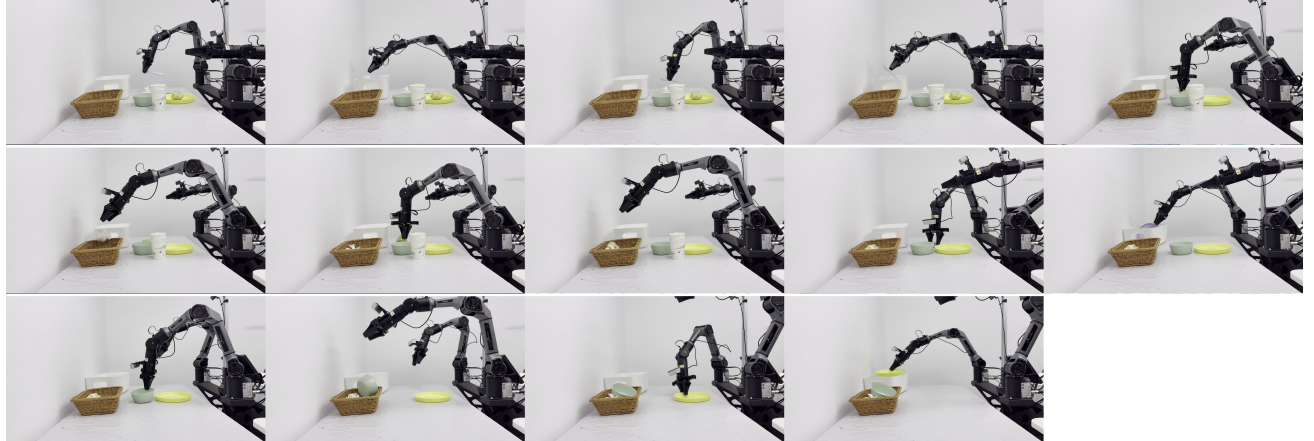


Figure 12. Additional visualization.

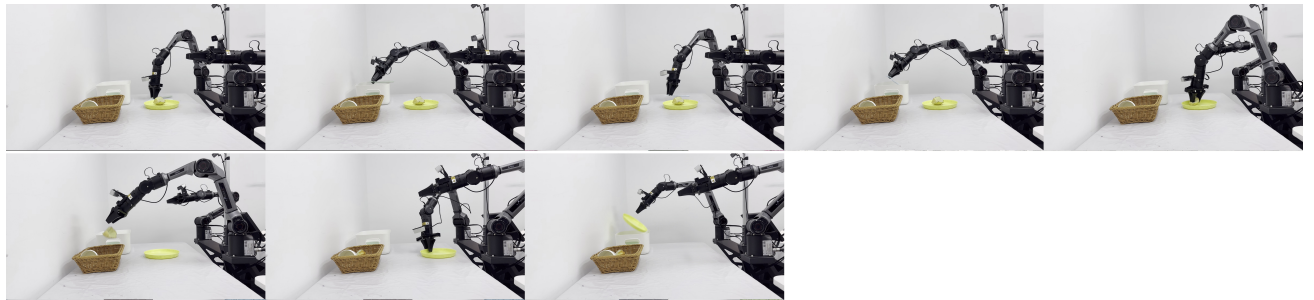


Figure 13. Additional visualization.

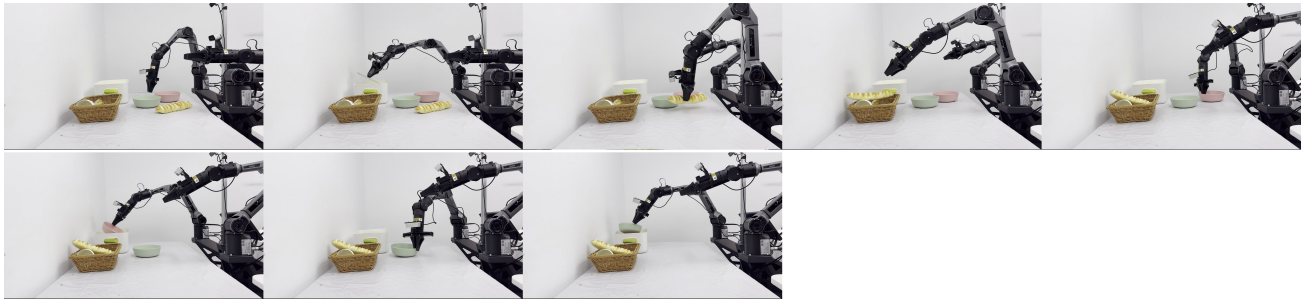


Figure 14. Additional visualization.



Figure 15. Additional visualization.

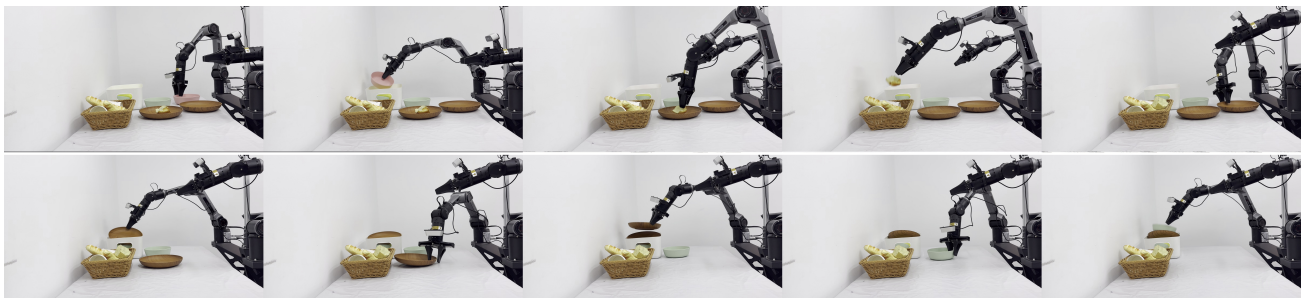


Figure 16. Additional visualization.

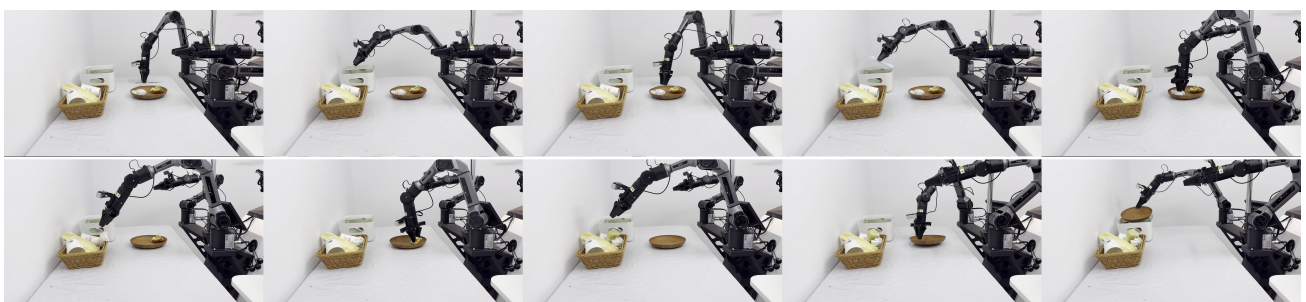


Figure 17. Additional visualization.

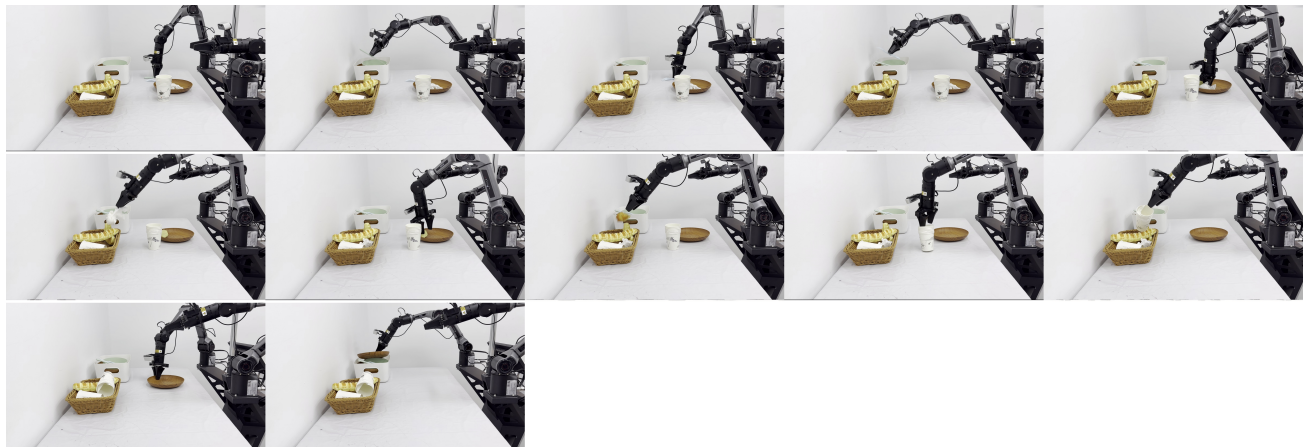


Figure 18. Additional visualization.